Evidence that excess ^{210}Pb flux varies with sediment accumulation rate and implications for dating recent sediments

José-María Abril , Gregg J. Brunskill

Abstract Most ^{210}Pb dating models assume that atmospheric flux of excess ^{210}Pb (^{210}Pb$_{exc}$) to the sediment–water interface remains constant over time. We revisited this assumption using statistical analysis of a database of laminated sediments and evaluated the implications for radiometric dating of recent deposits. A bibliographic survey enabled us to create a database with 10 annually laminated sediment cores from a variety of aquatic systems. The database has records of ^{210}Pb$_{exc}$ flux, initial ^{210}Pb$_{exc}$ activity, and sediment accumulation rate (SAR). ^{210}Pb$_{exc}$ flux to sediments varied with time, and 1/3 of the data had relative deviations from the mean value >25 %. There was no statistically significant correlation between activities at the core top and SAR, whereas a statistically significant ($p < 0.01$) linear regression between ^{210}Pb$_{exc}$ flux and SAR was found for nine of the ten cores. Thus, in most of the studied aquatic systems, ^{210}Pb$_{exc}$ flux to the sediment was governed primarily by flux of matter, rather than by direct atmospheric ^{210}Pb$_{exc}$ deposition. Errors in chronology and SAR, attributable to varying ^{210}Pb$_{exc}$ flux and estimated by the constant rate of supply (CRS) model, were evaluated from its analytical solutions, and tested against SAR values from this database that were derived independently from varves. We identified several constraints for general application of the CRS model, which must be taken into account to avoid its misuse.

Keywords Constant rate of ^{210}Pb supply model · Radiometric sediment chronology · Sediment accumulation rate · Time-dependent fluxes

J.-M. Abril (✉)
Departamento de Física Aplicada I, Universidad de Sevilla, Seville, Spain
e-mail: jmabril@us.es

G. J. Brunskill
84 Alligator Creek Road, Alligator Creek, QLD 4816, Australia
e-mail: g.brunskill@aims.gov.au

Introduction

Radiometric chronologies for recent sediment cores are thought to provide reliable estimates of sediment accumulation rate (SAR) and deposition processes, which are the key for inferring past environmental conditions. The most common technique for dating recent sediments uses fallout ^{210}Pb, a natural radionuclide. The method was proposed for dating glacier ice (Goldberg 1963) and was first applied to lacustrine sediments by Krishnaswamy et al. (1971), and to marine sediments by Koide et al. (1972). Use of this method increased rapidly and it was applied to a broad range of environmental studies. Over time, models for

sediment mass accumulation rate increased in variety and complexity (Robbins and Edgington 1975; Robbins et al. 1977; Appleby and Oldfield 1978; Christensen 1982; Abril et al. 1992; Caroll and Lerche 2003).

These models are predicated on a set of assumptions about the functioning of the studied sedimentary system, e.g. whether inputs of $^{210}Pb_{exc}$ and/or SAR are constant or time-dependent, or if diffusion is or is not relevant. These assumptions enable specific solutions for the depth-distribution of particle-associated radionuclides in sediments that have undergone accretion and compaction (Abril 2003a, 2011). To define the problem mathematically, initial and boundary conditions must be specified. Continuous flux at the sediment–water-interface (SWI) is imposed as a typical boundary condition, although in sediment with very high porosity, this assumption could be unrealistic (Abril and Gharbi 2012).

Continuous, constant flux of $^{210}Pb_{exc}$ to the SWI, along with the absence of post-depositional redistribution, constitute the basis for the constant rate of supply (CRS) model (Appleby and Oldfield 1978). When constant $^{210}Pb_{exc}$ flux persists over a century, the total inventory achieves steady state, i.e. flux at the SWI compensates for radioactive decay in the existing inventory. The restrictive hypothesis of steady-state profiles is common in most ^{210}Pb models because it enables analytical solutions (Robbins 1978). Thus, the assumption of constant $^{210}Pb_{exc}$ flux has been widely applied to a variety of aquatic systems, including lakes (Robbins and Edgington 1975; Appleby et al. 1979; Abril 2003b; Trabelsi et al. 2012), estuaries (Di Gregorio et al. 2007; Díaz-Asencio et al. 2009), and coastal areas and marine environments (Emeis et al. 2000; Zaborska et al. 2008). A variety of models accommodate non-post-depositional redistribution (Stevenson and Battarbee 1991; Appleby 2001), constant diffusion (Laissaoui et al. 2008), complete or incomplete mixing (Robbins et al. 1977; Abril et al. 1992; Abril 2004), translocation (Smith et al. 1986), and non-ideal deposition (Abril and Gharbi 2012). Most of these models also assume relatively constant SAR, which almost never happens. Some ^{210}Pb and bomb fallout profiles clearly suggest large variations in SAR, with consequent disruptions in profiles of radionuclides in the core.

A time-averaged century-scale $^{210}Pb_{exc}$ inventory and/or flux can be obtained from carefully chosen soil profiles in the vicinity of the lake, where soil is not rapidly eroded or deposited (Nozaki et al. 1978). This soil-derived value is almost always smaller than the inventory and average flux of $^{210}Pb_{exc}$ measured in the sediment of deep, bowl- or cone-shaped lake basins, because of focusing or funnelling of fine particles in the aquatic system. Although there is wide observational support for the constancy of annually averaged ^{210}Pb concentration in the lower atmosphere (von Gunten and Moser 1993), the deposition rate of atmospheric ^{210}Pb is influenced largely by rainfall, leading to large annual variations (30–50 %) in measured $^{210}Pb_{exc}$ deposition (Turekian et al. 1977; Rangarajan et al. 1986). Winkler and Rosner (2000) reported more than two-fold inter-annual variations. Thus, even in the simplest case of a water body for which $^{210}Pb_{exc}$ input is limited to direct fallout, the rate of supply is not constant over time. Catchment-derived sediment input can provide an additional supply of $^{210}Pb_{exc}$, which will vary from year to year in response to rainfall and land erosion, extreme events and changing land use, etc. Consequently, $^{210}Pb_{exc}$ flux to the SWI is controlled by the proportion of sediment supplied by each source, which is expected to vary over time. The assumption of constant flux used in many radiometric dating models needs to be applied with care and validated. In general, we expect that $^{210}Pb_{exc}$ activity will be high at the core top, and decline exponentially to supported ^{226}Ra values at sediment depths (i.e. ages) equivalent to 4–5 half lives of ^{210}Pb (22.26 years). Sediment depths of relatively constant $^{210}Pb_{exc}$ activity might be interpreted as zones of sediment and radionuclide mixing, or episodic supply of sediment with uniform activity, such as a turbidite, dust event or landslide.

Applying a subjectively chosen model without independent validation may lead to misleading results (Smith 2001). Any dataset with a $^{210}Pb_{exc}$ profile can be explained by multiple models, leading to different chronologies and SAR histories. Even in the case of a well-defined exponential $^{210}Pb_{exc}$ decrease, the profile can be explained under the hypothesis of constant flux by models involving constant SAR (with or without uniform and constant diffusion), or a constant increase of SAR over time, without diffusion. Independent validation is often accomplished by comparing ^{210}Pb model performance against chronology determined using artificial fallout radionuclides such as ^{137}Cs, ^{241}Am or $^{239,240}Pu$ (Klaminder et al. 2012), though

there are constraints for use of this technique (Abril 2003b, 2004).

A ^{210}Pb-based chronology can be plotted as a curve in the age versus depth plane, with a time marker such as a ^{137}Cs peak, tephra, etc., as a point in such a plane (with associated uncertainties). Quite often a ^{210}Pb-based chronology is considered validated when the age-depth curve adequately matches a single, independent time marker. Furthermore, the single time marker can be used to force a chronology, i.e. the curve is forced through the point, as with the reference-point method used to force the CRS model (Appleby 2001). In this last case, the assumption of constant flux is accepted implicitly rather than validated independently. Although this seems reasonable, many times the chronological results are questionable. Thus, in general, there is a lack of evidence about the reliability of these methods in validating/constructing chronologies in sediment cores for which there is an independent, high-resolution chronology, as is true for varved (i.e. annually laminated) sediments.

A varve-based chronology can only be established when the structure and annual nature of the varves is clearly understood and documented (Ojala et al. 2012). Not all laminated sediments are varved, and some laminated sediments are produced by achronologic, episodic pulses of sediment from within the lake and/or from the watershed (Wolfe et al. 1994). Once varve verification has been accomplished, such varved sediments are ideal for testing the validity of radiometric chronology models. Koide et al. (1973) studied a varved sediment core from Santa Barbara Basin and provided empirical evidence that the $^{210}Pb_{exc}$ activities decreased exponentially with time, as expected from the radioactive decay law and a constant (averaged) SAR.

Appleby et al. (1979) studied three varved sediment cores from lakes in east Finland and provided empirical validation of the CRS model in scenarios with varying SAR. But empirical evidence of the model's limitations has also been reported from the study of varved sediments. Wan et al. (1987) studied a varved sediment core from Greifensee Lake (Switzerland) and found that the depth of the 1963 activity peak for artificial fallout isotopes agreed with the varve chronology, whereas dates derived from ^{210}Pb analysis did not. Similar results were reported by Reinikainen et al. (1997) for varved sediments from Lakes Hankavesi and Vesijärvi, in central Finland, that had well-preserved ^{137}Cs peaks. Disagreement between CRS and varve dates was also found by Lamoureux (1998) in varved sediments from Nicolay Lake, Cornwall Island, Nunavut, Canada; by Chutko and Lamoureux (2009) in a bio-laminated freshwater lake in the Colin Archer Peninsula, Devon Island, Canada; by Finsinger et al. (2006) in a core from Lago Grande di Avigliana (northern Italy); and by Tylmann et al. (2013) in two cores from Lake Łazduny, northern Poland. In other cases, reasonable agreement was found between ages from the CRS model and the varve chronology (Lima et al. 2005—Pettaquamscutt River; Shanahan et al. 2008—in Lake Bosumtwi, Ghana).

These apparently contradictory results highlight the need to further explore $^{210}Pb_{exc}$ flux into the SWI, how flux variability limits the application of models that assume flux constancy, and to what extent the reference point method can be used to reliably test and correct for this situation. To address these issues, we used published data on laminated sediment cores taken from a variety of aquatic systems, which enabled us to build a database of records of SAR and $^{210}Pb_{exc}$ flux to the SWI. The database allowed a statistical analysis of the variability of ^{210}Pb flux with time, and its relationship with SAR values. The effects of such variability on CRS dates and SAR values are discussed using analytical solutions and case studies from this database. A lack of post-depositional mobility of particle-bound tracers in the varved sediments was assumed, as was continuous flux of $^{210}Pb_{exc}$ to the SWI. The purpose of this study was to evaluate the limitations of the constant-rate-of-supply (of $^{210}Pb_{exc}$) assumption, which, along with the above ones, defines the CRS model.

Materials and methods

Creation of a database with varved sediment cores

A systematic search was conducted with the ScienceDirect database (http://www.sciencedirect.com/), using "laminated sediments + 210-Pb" as the search criterion. The search yielded 708 results, 200 of them with "varve" in the text. All the papers and the references therein were carefully reviewed in the search for suitable data. This literature survey was complemented with a detailed review of ~140 papers in the varved-sediment database compiled by Ojala et al. (2012). Most of the papers did not allow for reliable data recovery. Only

nine sediment cores fulfilled the requirements for this work. Relevant data are summarized in Table 1 and Appendix A. They contain 144 lines of data with values for ages, SAR, and $^{210}Pb_{exc}$ concentrations.

The database (Electronic Supplementary Material [ESM]—Appendix A) contains sediment cores from Koide et al. (1973) and Wan et al. (1987) (C1 and C2, respectively; Table 1), briefly referred to in the Introduction. Two other varved cores (C4 and C5, respectively) came from Lakes Hankavesi and Vesijärvi, central Finland (Reinikainen et al. 1997). The authors calculated $^{210}Pb_{exc}$ flux to the sediment and found large temporal variability. Lima et al. (2005) studied a varved sediment core (C6) from Pettaquamscutt River (Rhode Island, Northeast USA). The $^{210}Pb_{exc}$ activity versus depth profile displayed exponential decay, and the CRS and CIC (Constant Initial Concentration) models showed good agreement with the chronology derived from varves. Kerfoot and Robbins (1999) reported data for a varved sediment core (C3) from Lake Portage, near Lake Superior, where mining activities governed mass flux into the lake. The Isle Royale Mill reduced operations in 1920 and terminated discharges in 1947 (Kerfoot and Robbins 1999); consequently only data after 1950 were used for the present study. Schettler et al. (2006a) studied a varved sediment core (C7) from Lake Sihailongwan, northeast China, yielding a 200-year record of $^{210}Pb_{exc}$ flux. Tylmann et al. (2013) studied two varved sediment cores from Lake Łazduny, northeast Poland, cores C8

Table 1 Database with varved sediment cores

Core/Ref.	Site and date of collection	Other tracers	^{210}Pb atmospheric fallout (Bq m^{-2} year^{-1})
C1/[1]	Santa Barbara Basin; 34°14.0′N, 120°01.5′W; 575 m depth. 1971. *Varves*: annual designations are based on a direct correlation of sediment thickness and rainfall for the past 100 years (Koide et al. 1972)	–	–
C2/[2]	Greifensee Lake (Switzerland); 47°21′N, 8°40′E; 24 m depth. October 1984. *Varves*: organic-rich ooze (dark laminae) and calcite precipitation (light laminae) during spring/early summer	^{137}Cs, ^{239,240}Pu, ^{90}Sr, ^{7}Be	143 [2]
C3/[3]	Portage Lake (Nearshore Regions of Lake Superior); 47°06′N, 80°30′W; 10–14 m depth. The fall of 1991. *Varve-like* slime clay layers associated with mining discharges	Heavy metals	~74 [7]
C4/[4]	Hankavesi Lake (Central Finland), 62°36′N, 26°45′E; 43 m depth. October 1995. *Varve* model not reported	^{137}Cs	55 ± 19 [6]
C5/[4]	Vesijärvi Lake (Central Finland), 61°31′N, 24°07′E; 39 m depth. October 1995. *Varve* model not reported	^{137}Cs	55 ± 19 [6]
C6/[5]	Pettaquamscutt River basin (Rhode Island, Northeast USA), 41°30′N, 71°26′W; 19.5 m depth. April 1999 *Varves*: biogenic and clastic layers	^{137}Cs	~120 [8]
C7/[9]	Sihailongwan Lake (Northeast China, Jilin Province), 42°17′N, 126°36′W; 50 m depth. September 1999. *Varves*: biogenic and clastic layers	^{137}Cs, ^{241}Am	>250 [9]
C8-C9/[10]	Lake Łazduny (northern Poland), 53°51.40′N, 21°57.30′E; 20–20.5 m depth. Collected in the years 2006 (C8) and 2007 (C9). *Varves*: regular succession of autochthonous calcite layers and organic-rich layers	^{137}Cs	110–130 [10]
C10/[11]	Fayetteville Green Lake (New York, USA), 43°03′N, 75°58′W; below 20 m depth. 1967. *Varves*: calcite precipitation in summer, and organic matter, clays and calcite deposited from fall to spring. Separated sampling of varves and turbidites	^{137}Cs	167 [12]

[1] Koide et al. (1973); [2] Wan et al. (1987); [3] Kerfoot and Robbins (1999); [4] Reinikainen et al. (1997); [5] Lima et al. (2005); [6] El-Dahoushy (1988); [7] Robbins and Edgington (1975); [8] From Appleby (1998) and annual rainfall data; [9] Schettler et al. (2006a); [10] Tylmann et al. (2013); [11] Brunskill and Ludlam (1988); [12] Graustein and Turekian (1986)

and C9 in the present compilation (Table 1). The authors applied multiple methods to estimate age, including varve counting, OSL, ^{137}Cs and ^{210}Pb dating, and tested different ^{210}Pb dating models against the varve chronology. More recently, they revisited the varve chronology for core C9 (Tylmann et al. 2014). Cores from Fayetteville Green Lake, studied by Brunskill (1969), Brunskill et al. (1984), Ludlam (1974, 1984) and Brunskill and Ludlam (1988), enabled distinguishing between contributions to SAR and $^{210}Pb_{exc}$ flux due to regular varves and turbidites. Core C10 (Table 1 and ESM Appendix B) serves to complete our analysis.

Authors used different image-analysis methods for varve counting, sometimes involving twin cores, and for establishing age-depth relationships, which were used to ascribe ages to either the mid-point or lower boundary of each sediment interval. Associated uncertainties were generally not reported. The reader is referred to the original publications for details. Measurement errors, however, can bias statistical analysis (Akritas and Bershady 1996) and must be included. Age errors associated with varve counting are typically <2 % (Lima et al. 2005; Schettler et al. 2006a). Errors in initial activity, A_0, are associated predominantly with radiometric measurement. Error information was available for all cores except C7, which was measured by alpha spectrometry and for which relative uncertainties of 5 % were assumed. Mass thickness can be measured with typical relative uncertainties <5 %, whereas relative errors in Δt depend on the number of varves included in each slice and their resolution. For simplicity sake, uniform relative uncertainties of 10 % were assumed for w (SAR) in this study. Exceptions were cores C8 and C9, for which the varve chronology uncertainties were reported, allowing for direct estimation of propagated errors. Statistical analysis was subjected to sensitivity testing to evaluate the effect of larger versus smaller SAR errors. Measurement errors of A_0 and w can be treated as being independent. Because F is obtained from the product w and A_o, its associated propagated error depends on the errors of w and A_o.

Data processing

In radiometric dating models, ^{210}Pb is assumed to be a particle-associated radionuclide, with negligible dissolved phases in the sediment pore water. When a mass flow, w (SAR), enters the SWI carrying $^{210}Pb_{exc}$ activity A_o, the associated $^{210}Pb_{exc}$ flux, F, is $F = wA_o$ (they are more properly "flux densities," but we use the term "flux" for simplicity). The assumption of constant flux over time necessarily implies co-variation of w and A_o.

Varved sediment cores allow reconstruction of historical SAR, initial concentrations and fluxes, through direct measurement in each sediment slice of age (varve chronology), activity of unsupported ^{210}Pb, thickness, and bulk density. Preservation of varves supports the assumption of negligible mobility of the particle-associated radionuclide, and activity profiles of bomb-fallout radionuclides or other environmental tracers with peaks at expected depths, provide additional support.

The methods used to reconstruct records of varve SAR and $^{210}Pb_{exc}$ flux can be found in the literature (Brunskill et al. 1984; Brunskill and Ludlam 1988; Ludlam 1984; Reinikainen et al. 1997; Kerfoot and Robbins 1999; Schettler et al. 2006a). Briefly, for a given sediment slice with mass thickness Δm (M L^{-2}) and an elapsed time between its lower and upper boundaries Δt (T), the mean SAR value for this time interval is $w = \Delta m/\Delta t$. If the measured $^{210}Pb_{exc}$ concentration in the slice is A (Bq M^{-1}), and the age of its upper boundary is t_{up} (T), the mean flux onto the SWI, F (Bq L^{-2} T^{-1}), assumed to be constant during the time interval Δt, and accounting for the radioactive decay with constant λ, can be estimated as follows:

$$F = Aw\frac{\lambda\Delta t}{[1-\exp(-\lambda\Delta t)]}\exp(\lambda t_{up}) \quad (1)$$

Initial activity, A_o, can be estimated by applying the correction for radioactive decay to the measured value of A; or, as the ratio F/w.

This approach allows for estimation of mean values over Δt, over which shorter-scale fluctuations are superimposed. But this is the operational definition for the measurable magnitudes that one can achieve in radiometric dating of recent sediments, and the statistical study that follows applies to them, along with their associated measurement errors. The effects of a discrete resolution and fluctuations are treated in the Discussion section.

Statgraphics Plus 5.1 and IBM SPSS software were used for adjusting distributions and for correlation analysis. The BCES estimator (Bivariate Correlated Errors and intrinsic Scatter) was used for linear

regression analysis (Akritas and Bershady 1996). BCES allows for measurement errors in both variables (errors can be dependent), and allows the magnitude of the measurement errors to depend on the measurements.

Results

Figures 1, 2 and 3 show the time series of $^{210}Pb_{exc}$ fluxes onto the SWI for the studied aquatic environments. These fluxes vary noticeably over the temporal range of the varve chronologies, and in all cases except cores C2 and C8 (Table 1), their values are much higher than expected from local atmospheric deposition (Table 1).

For each core, a second panel shows the $^{210}Pb_{exc}$ fluxes versus SAR. In all cases, a BCES linear relationship can be established at a confidence level (CL) of 99 %. The independent terms (ordinate at origin) in the linear fits were compatible with zero, considering associated uncertainties, the slopes (Bq M^{-1}) being related with the initial $^{210}Pb_{exc}$ activities. Fluxes and SAR surpassed normality tests, except fluxes in core C2, (ESM Appendix C).

For core C7 (Lake Sihailongwan, northeast China), the time series of $^{210}Pb_{exc}$ fluxes onto the SWI estimated in this work and that of Schettler et al. (2006a) are shown (Fig. 3). They coincide except in the three uppermost data points, the ones most affected by ice extrusion during the freezing of the core after sampling, and perhaps application of corrections not

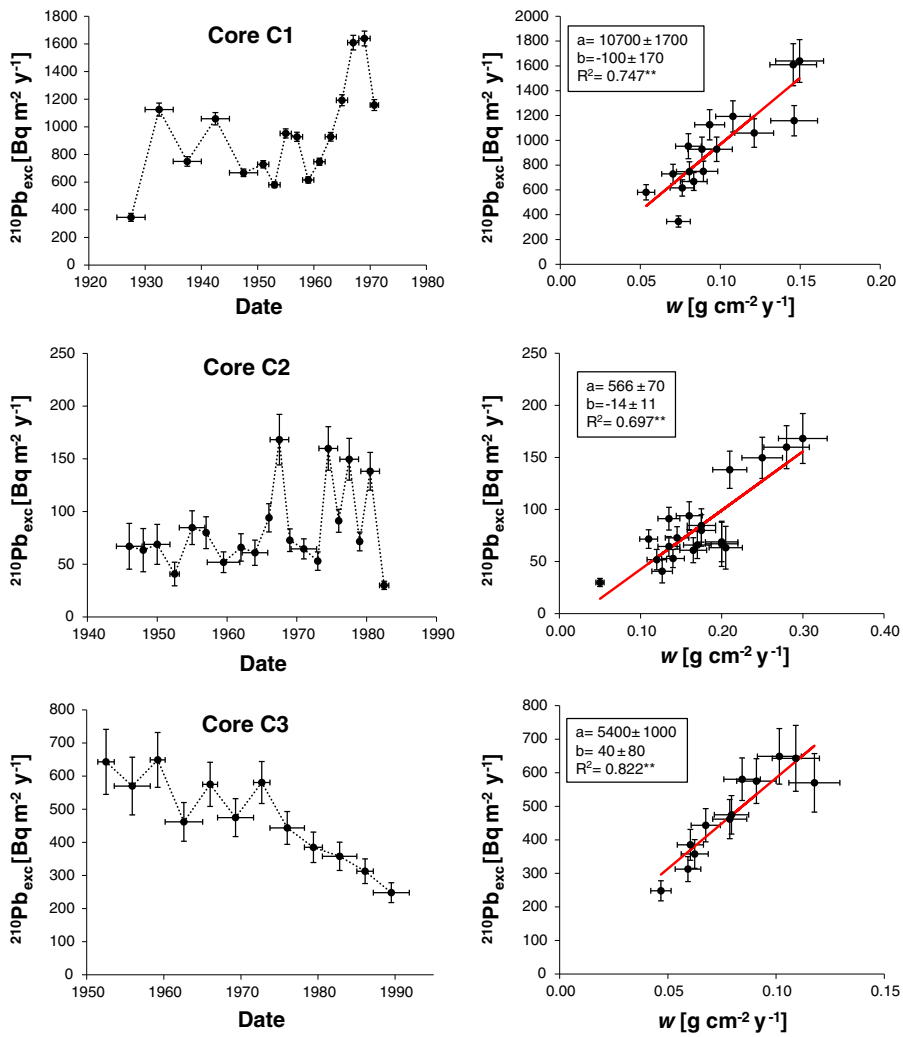

Fig. 1 Reconstructed time series of $^{210}Pb_{exc}$ fluxes onto the SWI (*left panels*); and $^{210}Pb_{exc}$ fluxes versus SAR values with linear BCES regression (*right panels*), for cores C1, C2 and C3 (see Table 1 and ESM Appendix A). Error bars correspond to 1σ. *Horizontal bars* in *left panel* define the time interval (from varves) associated with each sediment slice. In *boxes* "a" is the slope and R^2 the coefficient of determination; * and ** denote confidence levels greater than 95 and 99 %, respectively

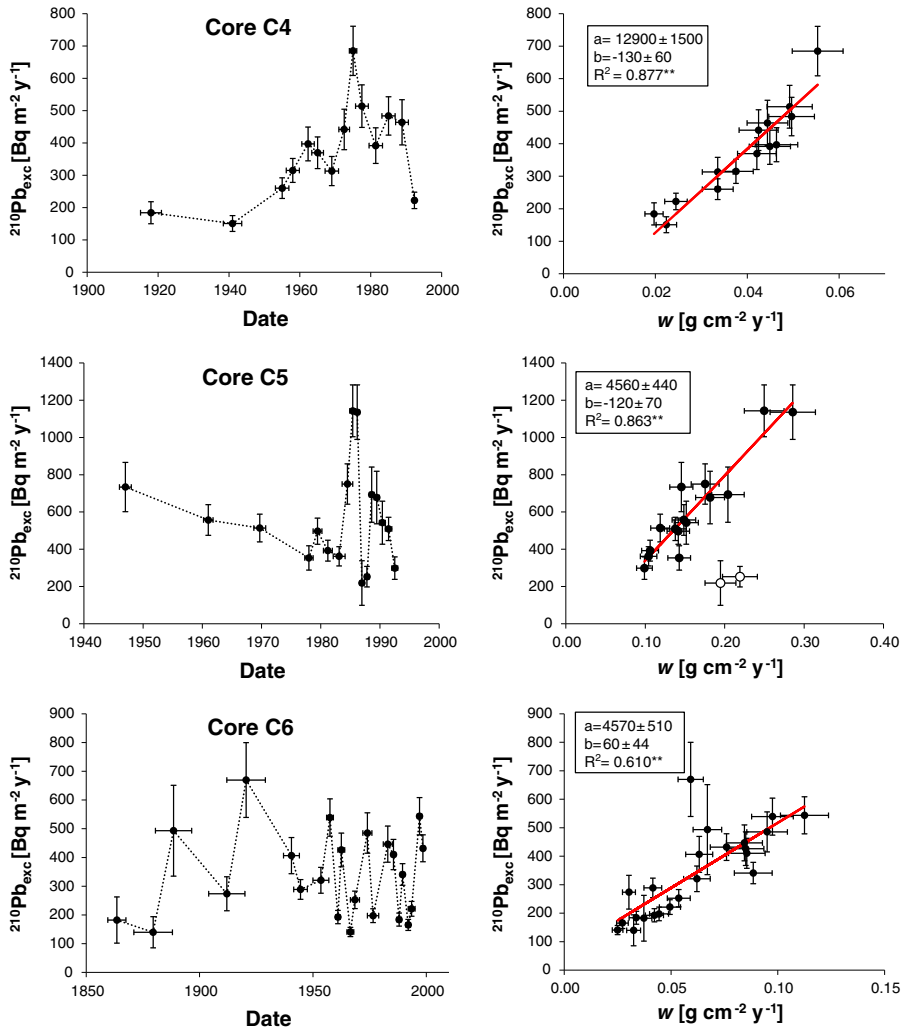

Fig. 2 As for Fig. 1, but for cores C4, C5 and C6 (see Table 1 and ESM Appendix A). *Open circles* in core C5 (*right panel*) were not included in BCES estimator

fully explained in the original paper. The BCES estimator omitted the data from slice number 5 (ESM Appendix A), which included several thick clastic layers, likely from episodic dust storms (Schettler et al. 2006b). The low $^{210}Pb_{exc}$ activity in this storm dust explains how an episodic event can cause data to fall outside of the expected trend (Fig. 3), which otherwise holds under most conditions.

Data on initial ^{210}Pb activities failed the normality test in most cases (ESM Appendix C). Thus, the bivariate correlation test of Pearson was applied for w and A_0 after data transformation (ESM Appendix C). Correlation was only statistically significant for core C4. A_0 was plotted versus w for all the cores (ESM Fig. A-1), along with results from the BCES estimator, which revealed the lack of a statistically significant regression.

For each core, the arithmetic mean of $^{210}Pb_{exc}$ fluxes ($\bar{F}$), $^{210}Pb_{exc}$ initial activities ($\bar{A}_0$) and SAR ($\bar{w}$) were derived from their respective time series, covering the range of the varve chronology, as shown for SAR values (ESM Appendix A). These arithmetic means were then used to create the corresponding normalized variables: e.g. for fluxes, $F_{norm}(i) = F(i)/\bar{F}$, where index (i) denotes the sediment slice. This way, it is possible to run a global statistical evaluation of the data. Figure A-2 (ESM) shows the corresponding histograms with the frequency distributions of normalized values, and normality tests are reported in ESM Appendix C.

Normalized $^{210}Pb_{exc}$ fluxes versus normalized SAR display a linear relationship (99 % CL, $R^2 = 0.744$) with a slope of 1.00 ± 0.06 and the ordinate at the origin, 0.00 ± 0.06 (Fig. 4). Normalized $^{210}Pb_{exc}$

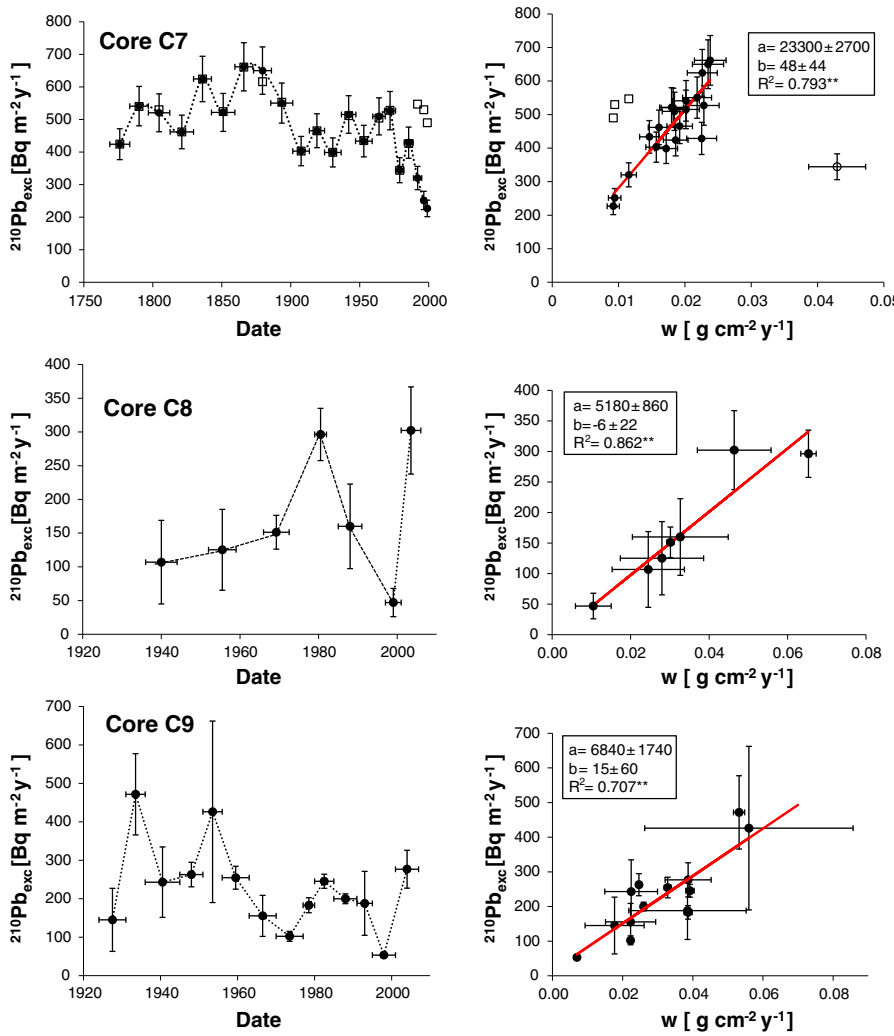

Fig. 3 As for Fig. 1, but for cores C7, C8 and C9 (see Table 1 and ESM Appendix A). For core C7 *open squares* are fluxes estimated by Schettler et al. (2006a)—see the text for the origin of discrepancies in the three uppermost data points, and the *open circle* corresponds to slice number 5, most likely affected by a dust storm event (*open circle* in *right panel*, not included in BCES)

fluxes were also linearly related with normalized concentrations (not shown) at 95 % CL ($R^2 = 0.23$, slope 0.98 ± 0.36, ordinate at the origin, 0.02 ± 0.36; results from BCES estimator). When the residual values of normalized fluxes (i.e. their deviations from the BCES linear fit in Fig. 4) are plotted against the normalized concentrations, as done in the last panel of Fig. 4, a BCES linear regression explains 92 % of their variability. The BCES regression for F and w was re-evaluated using relative uncertainties of 5 and 15 % for w for cores C1 to C7, but maintaining values for cores C8-C9, and updating the propagated errors in F. Results remained essentially unchanged within the associated uncertainties in the regression parameters, and changes in slope were <1 %.

Data from Core C10 (Fig. 5 and ESM Appendix B) required a different treatment because they came from a different method that allowed distinguishing between contributions to SAR and $^{210}Pb_{exc}$ fluxes from varves and turbidites (Brunskill et al. 1984; Brunskill and Ludlam 1988). They are treated in the Discussion section.

Discussion

Initial $^{210}Pb_{exc}$ activities (A_0) versus SAR

Neither the bivariate test of Pearson nor the BCES estimator revealed any statistically significant relationships between A_0 and SAR, except for core C4

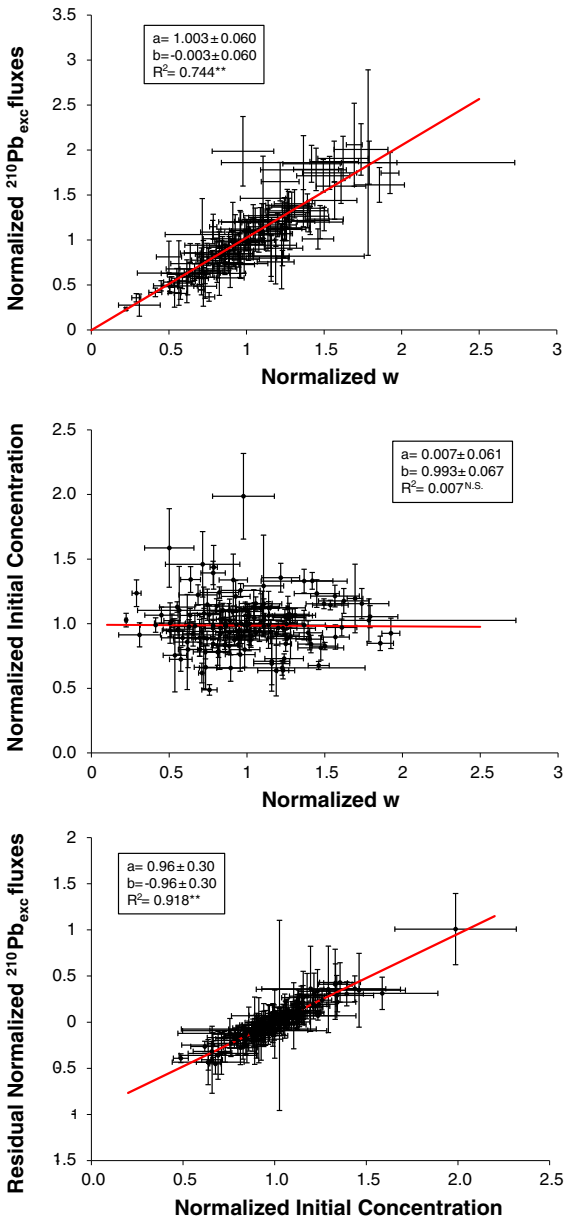

Fig. 4 Normalized $^{210}Pb_{exc}$ fluxes and initial activities versus normalized SAR, and linear BCES regression for cores C1 to C9. The last panel plots residual values (deviations from measurements and the BCES predictions) of the normalized fluxes versus normalized initial activities, along with the BCES linear regression

(Fig. A-1 and ESM Appendix C). This suggests that initial concentrations were governed mainly by the $^{210}Pb_{exc}$ fraction that particulate matter carries from the catchment and/or from other sites in the aquatic environment, through resuspension and re-deposition. Variability in values for initial activity could be driven principally by changes in the intensity of inputs from different erosional areas under varying meteorological conditions and/or human activities, along with natural variability in atmospheric deposition (Winkler and Rosner 2000) and the mineralogical composition and particle size distribution of the deposited matter (Abril and Fraga 1996). The expected outcome from the hypothesis of constant rate of supply of $^{210}Pb_{exc}$ is constant flux, and initial activity decreasing with increasing SAR. For core C4, changes in SAR explained 1/3 of the variability in A_0, the increasing trend likely a consequence of the contribution to the mass flow of particulate matter with relatively higher activity. In Fig. 5, initial activity of ^{210}Pb declines with increasing SAR, because nearly all the varve sediment is created within the lake water column (Brunskill 1969; Brunskill and Ludlam 1988), and variation in measured ^{210}Pb flux at the deep-water SWI is small.

$^{210}Pb_{exc}$ fluxes to the SWI versus SAR

In summary, in most of the studied aquatic environments the $^{210}Pb_{exc}$ fluxes were time-dependent, with one third of the data showing relative deviations with respect to the mean value >25 %. The BCES method revealed a statistically significant (at 99 % CL) linear regression between F and w for all the cores and for the whole set of normalized data. Approximately 2/3 of the variability in $^{210}Pb_{exc}$ flux is linked to variability in SAR, and 1/3 to variability in initial activity, these last two being uncorrelated variables. This result is clearly opposite to the assumption of constant $^{210}Pb_{exc}$ flux.

Taking into account seasonal variability and the time scales involved in radiometric dating of recent sediments, meaningful definitions of F and w require averaging over time intervals on the order of several years to decades. It is worth noting that the relationships in Figs. 1, 2, 3 and 4 apply to values of F and w averaged over the varying time intervals Δt_S (on the order of several years) associated with each sediment slice. By definition, the averaged value over Δt_S of any meaningful shorter-scale fluctuations of these magnitudes around their respective mean values (over Δt_S), must be zero.

Appleby (2001) reported a statistically significant negative correlation between surficial $^{210}Pb_{exc}$ activity and mean SAR during the past 75 years in a large set

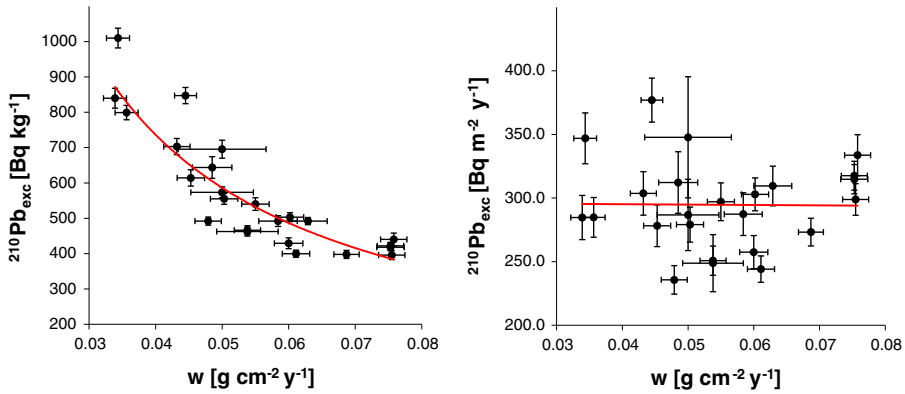

Fig. 5 Initial $^{210}Pb_{exc}$ activities and fluxes versus SAR for the Fayetteville Green Lake core (data from Brunskill and Ludlam 1988) with 1-σ *error bars*. Data correspond to the contribution of the varve material, which was sampled separately from turbidites. Trend *lines* are also depicted

of sediment cores from lakes in England, Ireland, Scotland, Cumbria and Wales. Activity decreased with SAR, which seems to contradict our results. In the study of Appleby (2001), different lacustrine environments that receive similar fallout $^{210}Pb_{exc}$, showed different abilities to capture the radioisotope and transfer it to the sediments. In this inter-lake comparison, the greater the flow of matter (i.e. sedimentation), the lower the activity of the particulate matter. This provided valuable insights into the behavior of ^{210}Pb in the environment. Within a particular sedimentary basin, however, we found temporal variability in SAR (around the mean value), and independent variability in initial ^{210}Pb activity, which suggests time-dependent changes in $^{210}Pb_{exc}$ fluxes. This provided information about the behavior of $^{210}Pb_{exc}$ flux onto the SWI in a particular aquatic environment, the question that is relevant for sediment core chronological models. Normalization to the local mean values enabled comparison of different aquatic systems, and we found a significant positive correlation between $^{210}Pb_{exc}$ flux and SAR in cores C1 to C9. A few data, for instance slice 5 in core C7, showed an atypical departure from the linear relationship between $^{210}Pb_{exc}$ flux and SAR that holds under most environmental conditions, and this was attributed to an extreme, episodic event.

Fayetteville Green Lake varves and turbidites

Brunskill (1969), Ludlam (1969, 1981), Brunskill et al. (1984) and Brunskill and Ludlam (1988) studied laminated sediment cores from Fayetteville Green Lake (Table 1). They showed thin, light and dark colored lamina couplets (varves) that were linked to inorganic calcite precipitation in summer, and to organic matter, clay and calcite deposition in winter, respectively. Varve sedimentation was irregularly supplemented with nearshore sediments, spread by turbidity currents that formed coarse-grained sediment layers referred to as turbidites by the authors. The method used by Brunskill and Ludlam (1988) and Brunskill et al. (1984) allowed separate sampling and radionuclide analysis (^{210}Pb and ^{137}Cs) of varve layers and turbidites. They quantified the contribution to mass accumulation (SAR) associated with varves, with variations largely a consequence of differences in the thickness of the summer calcite lamina. Using the varve chronology, the authors were able to estimate the initial $^{210}Pb_{exc}$ activity for each varve. The data show a trend of decreasing $^{210}Pb_{exc}$ activity with increasing varve SAR (Fig. 5). Furthermore, reconstructed $^{210}Pb_{exc}$ flux onto the SWI inferred from varves was almost constant, with a mean value of 296 Bq m^{-2} year^{-1} and a standard deviation of 12 % (Fig. 5). This is in good agreement with the assumption of constant $^{210}Pb_{exc}$ flux in the CRS model, and seems to contradict our present results. Nevertheless, this method only accounted for $^{210}Pb_{exc}$ scavenged by processes associated with varve formation, and excluded the contribution to flux onto the SWI from excess ^{210}Pb associated with turbidites. Distinguishing these two sources can improve insights into $^{210}Pb_{exc}$ flux and its relationship with SAR.

A two-component mass flow model with intrinsic scatter

The empirical results from cores C1 to C10 can be understood using a simple two-component mass flow model (and associated $^{210}Pb_{exc}$ inputs), with intrinsic scatter. Let w_V and F_V be the fluxes of matter and $^{210}Pb_{exc}$, respectively, linked to the "vertical scavenging" in the water column of $^{210}Pb_{exc}$ coming primarily from fresh meteoric fallout. These are averaged values over the varying time intervals Δt_S (on the order of several years) associated with typical sediment slices. These magnitudes show natural and, at a first, independent variability (δF_V, δw_V) around their mean values ($\bar{F}_V, \bar{w}_V$) over decadal time scales. Atmospheric deposition primarily governs the $^{210}Pb_{exc}$ in the water column, where it is scavenged by organic matter and settling inorganic particles under a low-energy regimen. Nyffeler et al. (1984) and Honeyman and Santschi (1989) describe the process of radionuclide sorption by particulate matter and its scavenging, mediated by the coagulation of colloids. The ^{210}Pb activity in scavenged material, A_V, will be

$$A_V = \frac{F_V}{w_V} = \frac{\bar{F}_V}{w_V}\left(1 + \frac{\delta F_V}{\bar{F}_V}\right). \quad (2)$$

Figure 6 shows a numerical exercise that includes random variations in normalized w_V and F_V. One hundred values were generated using the Microsoft Excel random number generator, achieving a normality distribution and standard deviation of 0.25 and 0.125, respectively. The corresponding initial concentrations estimated from Eq. 2 follow a pattern of decrease with w_V, as observed in core C10. Other contributions to the mass flow and $^{210}Pb_{exc}$ fluxes include catchment-derived sediments, which are generally delivered to the SWI by slow sedimentation, sediment redeposition within the lake basin from focusing or other processes, and sediment deposits associated with turbidity currents. Such sediments are

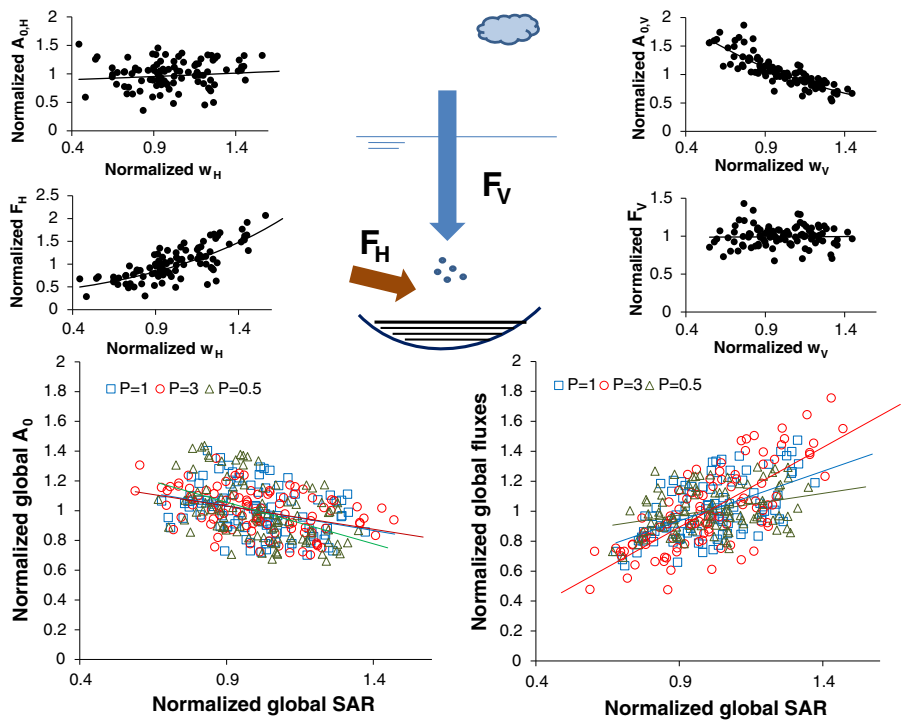

Fig. 6 The two-component mass flow model with intrinsic scatter. Random variations around mean values of fluxes of scavenged $^{210}Pb_{exc}$, F_V, and the associated mass flows, w_V, lead to initial activities, A_V, that decrease with increasing w_V. Horizontal inputs from the catchment and other areas within the lake are characterized by initial activities, A_H, and mass flows, w_H, with random variations around their mean values, which lead to fluxes, F_H, increasing with w_H. Superposition of both signals, which are simultaneous in terms of typical time-scales, but with different relative intensities, $P = F_H/F_V$, results in the relationships between global initial activity and global flux versus global SAR depicted in the lower panels

simply referred to here as "horizontal inputs," and are characterized by their mean values, $\bar{w}_H$ and $\bar{A}_H$ (over the same Δt as the vertical inputs), and random and independent variability (δw_H , δA_H). A set of 100 normalized values were randomly generated, as in the previous case, with equal standard deviations of 0.25 for both magnitudes. The associated $^{210}Pb_{exc}$ inputs can be estimated as $F_H = A_H w_H$, and then renormalized. This leads to a trend of increasing F_H with increasing w_H (Fig. 6).

Within the time resolution Δt_S, both signals overlap. Their relative contribution can be characterized by the ratio $P = \bar{F}_H/\bar{F}_V$. For the sake of simplicity, in this conceptual model we adopt $\bar{A}_H = \bar{A}_V$. Global or composited magnitudes, without separation of solid particles by origin, are commonly used in radiometric dating of recent sediments: $F_G = F_H + F_V$; $w_G = w_T + w_V$, and the mass-averaged initial concentration,

$$A_G = \frac{A_T w_T + A_V w_V}{w_T + w_V}. \tag{3}$$

Results for normalized global A_G and F_G versus w_G were plotted for P values of 0.5, 1 and 3 (Fig. 6). As the P ratio becomes larger, horizontal inputs become dominant, leading to a lack of correlation between A_G and SAR and a trend of increasing F_G with increasing SAR.

Combined contributions from water-column processes and catchment and/or other areas within the aquatic ecosystem to the mass (SAR) and $^{210}Pb_{exc}$ flux to the SWI are common in both varved and non-varved sediments. When contributions from the watershed catchment area and/or turbidites become dominant, $^{210}Pb_{exc}$ fluxes increase with SAR. This was the situation for most of the studied cores, as deduced from $^{210}Pb_{exc}$ fluxes to SWI (Figs. 1, 2, 3), when compared to corresponding values of local atmospheric deposition (Table 1). Cores C2 and C8 are exceptions, with global flux being similar to or even lower than atmospheric deposition, but still linearly correlated with SAR. This situation can be interpreted as reflecting low efficiency of scavenging by meteoric fallout when compared to the contribution of horizontal inputs. Cores included in this work cover a variety of lacustrine environments from different regions of the world, a marine sediment core and a core from a river basin (Table 1). This provides support for the conclusion that $^{210}Pb_{exc}$ fluxes vary with time and increase with SAR when P is large, as found in most of the cases, but in some particular environments they can be less variable and decrease with SAR (when P is small).

Effect of varying flux on SAR and chronology estimated using the CRS model

If Σ_0 is the unsupported ^{210}Pb inventory below the SWI in a sediment core at time t = 0, the "equivalent steady-state flux" is defined as $F_e = \lambda\, \Sigma_0$. During the elapsed time Δt, a new flux, F, assumed to be constant during this time interval, will enter the SWI. The SAR during Δt, w, is assumed to be equally constant, i.e. Δt will be the maximum time interval during which F and w remain constant. We define the ratio k as $k = F/F_e$. Taking into account radioactive decay, the new total inventory Σ_0^* and the inventory below the former SWI, Σ_b^*, are, respectively:

$$\Sigma_0^* = \frac{F}{\lambda}[1 - \exp(-\lambda \Delta t)] + \Sigma_b^*; \quad \Sigma_b^* = \Sigma_0 \exp(-\lambda \Delta t)$$

From these two inventories, the CRS model (Appleby and Oldfield 1978) estimates an elapsed time

$$\Delta t_{CRS} = \frac{1}{\lambda} \ln \frac{\Sigma_0^*}{\Sigma_b^*} = \Delta t + \frac{1}{\lambda} \ln[k + (1 - k) \exp(-\lambda \Delta t)]$$

When $k = 1$, the basic assumption of the CRS model is met and then $\Delta t_{CRS} = \Delta t$. The mass thickness accumulated during the elapsed time is $w\Delta t$, and from that value, the CRS model estimates the following value for SAR:

$$w_{CRS} = \frac{w \Delta t}{\Delta t_{CRS}}.$$

Absolute deviations in chronology and sediment accumulation rates are

$$\delta_t = \Delta t_{CRS} - \Delta t; \quad \delta_w = w_{CRS} - w$$

Taking into account that for time intervals on the order of 1–2 years, $\lambda\Delta t$ is a small number, and first-order expansion allows estimation of the relative errors:

$$\varepsilon_{r,t} = \frac{\delta_t}{\Delta t} \cong k - 1$$
$$\varepsilon_{r,w} = \frac{\delta_w}{w} \cong \frac{1 - k}{k} \tag{4}$$

These relative errors in the chronological parameters ascribed to any given sediment slice are preserved in time. Thus, from Eq. 4, a variation of 30 % in flux, with respect to "equivalent steady-state values," leads to relative errors of 30 % in the elapsed time, and 23 % and 43 % in SAR when fluxes increase ($k = 1.3$) or decrease ($k = 0.7$), respectively. We refer here to "model errors" (the model does not appropriately reproduce the real scenario), which are different from measurement errors. The whole sediment core can be scanned from bottom to top using this method. Cumulative deviations in the chronology and in the averaged SAR tend to cancel out when they are purely random, but the situation can be different under persisting trends of increase or decrease in $^{210}Pb_{exc}$ fluxes, as discussed in the next section.

Constraints for the CRS model

In this section, we explore the cumulative error in chronology and SAR from the CRS model, when the time series of $^{210}Pb_{exc}$ flux (and SAR) follows a continuous trend of decrease or increase, as observed in core C1 from Santa Barbara Basin (Fig. 1).

Alternative dating models are applied to the $^{210}Pb_{exc}$ profile for core C1 (Fig. 7a):

1. The common approach neglects the uppermost part of the sediment, until the ^{210}Pb maximum is attained, and uses an exponential fit—continuous line (Fig. 7a). This is the constant flux-constant sedimentation rate (CF-CSR) model, which provides a SAR value of $w = 0.068 \pm 0.007$ g cm^{-2} year^{-1}.
2. Application of the stand-alone CRS model. As the measured inventory (23.7 kBq m^{-2}) is incomplete, i.e. there is still measured $^{210}Pb_{exc}$ activity, this value was corrected by extrapolation of the exponential pattern found in the deepest layers, leading to an inventory correction of 3.6 kBq m^{-2}. Model results produce a varying SAR, with a depth-averaged value of 0.069 g cm^{-2} year^{-1} and standard deviation 0.010 g cm^{-2} year^{-1}.
3. The reference-point method (1). Provided that the date of the deepest layer, T_d, is known (e.g. from varves in this case), it is possible to estimate the constant flux, F, required to produce the measured inventory Σ_m (from the SWI to the deepest layer): $\Sigma_m = F \int_0^{T_d} e^{-\lambda t} dt$. Assuming that this flux also holds for ages older than T_d, one can estimate the correction, Σ_c, which must be added to complete the inventory: $\Sigma_c = F \int_{T_d}^{\infty} e^{-\lambda t} dt$. Application to Core C1 leads to $\Sigma_c = 7.27$ kBq m^{-2} (30.7 % of

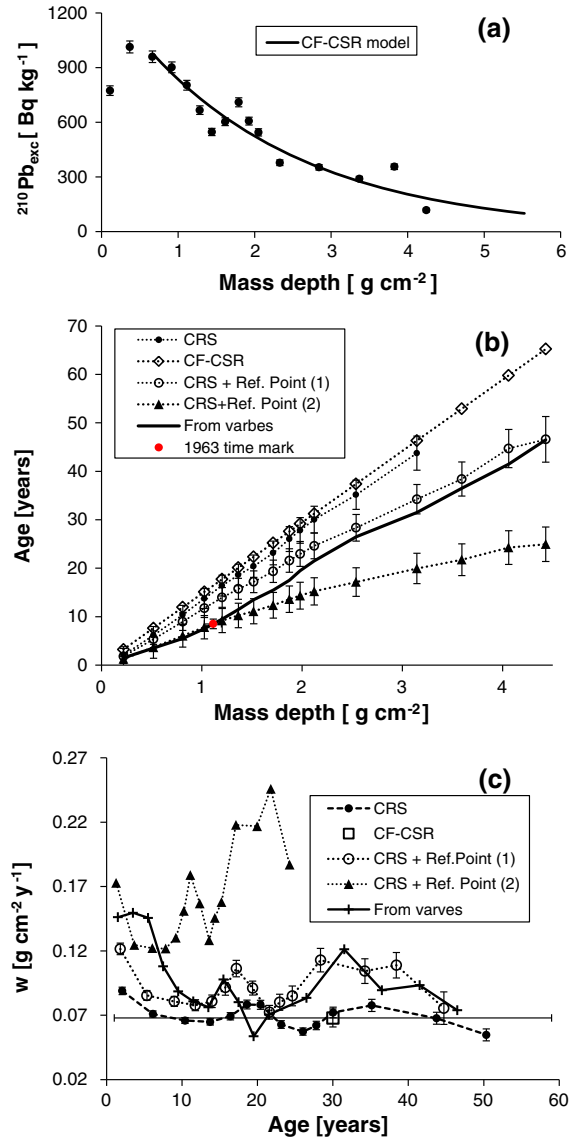

Fig. 7 **a** $^{210}Pb_{exc}$ versus mass depth profile for core C1 (Table 1 and ESM Appendix A, data from Koide et al. 1973) and the best exponential fit after omitting the two uppermost data points (CF-CSR model). **b** Chronologies obtained from varves, and from the CF-CSR, CRS, and CRS models, using the reference point method. **c** SAR versus ages obtained from varves and the previous models

Σ_m). After this correction, the CRS age of the deepest layer is $1/\lambda \ln[(\Sigma_m + \Sigma_c)/\Sigma_c) = T_d$. This way, the CRS chronology is "tied" to the true chronology from varves at two points, the SWI and the deepest layer. This method corresponds to the one used by Appleby et al. (1979).

4. The reference-point method (2). The CRS chronology is forced to match a reference time marker within the time scale, in this example the year 1963, in the layer 6.1–7.1 cm (ESM Appendix A). The partial inventory contained in this top layer requires a constant flux of 1,363 Bq m^{-2} $year^{-1}$.

Chronologies derived from these models can be compared with the chronology obtained from Santa Barbara basin varves (Fig. 7b). The stand-alone CRS and the CF-CSR models produce concordant chronologies and SAR histories (Fig. 7c), often considered sufficient support for establishing a radiochronology. Nevertheless, in this case the models do not pass the varve chronology test, and their SAR histories differ substantially from the one derived from varves (Fig. 7c). The CRS model with the reference-point method (1) produces a chronology that closely follows the one obtained from varves, and its SAR history reproduces roughly the main features registered by the SAR history from varves (Fig. 7c). Nevertheless, a significant disagreement between true and modeled ages is found in the lower part of the profile, where the reference point is the year 1963. We note that this version of the reference point method is the one used most commonly in radiometric dating of recent sediments.

As the authors demonstrated in their respective papers (Table 1), the CRS model failed to reproduce the varve chronologies of cores C2, C4, C8 and C9, yielded poor results for C7, and reasonable results for cores C6 and C5, the latter through the reference point method. The Sediment Isotope Tomography (SIT) model (Caroll and Lerche 2003) can be applied to situations with variable SAR and $^{210}Pb_{exc}$ flux, and seems to be a powerful tool. Tylmann et al. (2013) reported SIT chronologies consistent with varve dates for cores C8 and C9. It is worth, however, noting some limitations of the method. To constrain the infinite number of mathematical solutions, the SIT model requires the use of known time markers within the core (e.g. ^{137}Cs peaks), and, as demonstrated by Caroll and Lerche (2003) using synthetic $^{210}Pb_{exc}$ profiles, a single time marker in some cases (e.g. at shallow depth in a core) does not yield a reliable solution. Other assumptions of the SIT model, for instance absence of post-depositional redistribution, need independent validation (Abril 2004).

Conclusions

The compiled database of laminated sediment cores enabled reconstruction of a suitable set of historical records of $^{210}Pb_{exc}$ flux to the SWI, SAR and initial $^{210}Pb_{exc}$ activity. These three variables showed large temporal fluctuations, and there was no statistically significant correlation between initial activity and SAR, violating an assumption of most ^{210}Pb-based radiometric dating models. Furthermore, for $^{210}Pb_{exc}$ flux, the BCES method established a linear regression with SAR (99 % CL) that explained $\sim$2/3 of the observed variability in $^{210}Pb_{exc}$ flux for cores C1 to C9. Analysis of the Fayetteville Green Lake cores distinguished between contributions to SAR and $^{210}Pb_{exc}$ fluxes from water-column processes and fluxes of matter from the catchment and/or other areas within the system. When these latter sources dominate, a positive linear regression between $^{210}Pb_{exc}$ flux and SAR naturally arises. In the case of negligible horizontal inputs, as defined in this paper, such as in Fayetteville Green Lake, water-column processes dominate the scavenging of atmospherically derived $^{210}Pb_{exc}$ and variation in $^{210}Pb_{exc}$ flux is greatly reduced and $^{210}Pb_{exc}$ activities are inversely related to SAR. The number and diversity of aquatic systems studied here provides support for the claim that it is most common for $^{210}Pb_{exc}$ flux to vary and increase with SAR.

One third of the $^{210}Pb_{exc}$ flux data showed deviations from the mean value >25 %, which limits the value of chronologies and SARs obtained with the CRS model. From the analytical evaluation of associated errors and their cumulative effect, the following constraints on use of the model include:

(1) Similarities between chronologies and SAR histories produced by stand-alone CRS and CF-CSR models cannot be considered independent validation. (2) Non-monotonic $^{210}Pb_{exc}$ profiles have often been linked to conditions of varying SAR; because of the proved correlation between $^{210}Pb_{exc}$ flux and SAR,

application of the CRS model to this kind of profile should be undertaken with caution. (3) Use of reference points to constrain the CRS model can improve its performance, but such time markers constitute a unique dating tool, and results still require independent validation. These constraints do not apply to lakes with negligible horizontal sediment inputs, which appear to abide by the assumptions of the CRS model.

These constraints should be understood as a positive contribution to practical application of the CRS model, which will help avoid its inappropriate use. It remains a useful method for determining SAR and rough horizon ages, and without these dating tools, we would have no way to determine sediment accumulation rates or the history of deposition of microfossils, contaminants, and climate over the last century.

Acknowledgments This work was funded partially by the FIS2012-31853 Project. We sincerely acknowledge the excellent work carried out by the authors of the papers from which we constructed the database used in this study.

References

Abril JM (2003a) A new theoretical treatment of compaction and the advective-diffusive processes in sediments. A reviewed basis for radiometric dating models. J Paleolimnol 30:363–370

Abril JM (2003b) Difficulties in interpreting fast mixing in the radiometric dating of sediments using ^{210}Pb and ^{137}Cs. J Paleolimnol 30:407–414

Abril JM (2004) Constraints on the use of Cs-137 as a time-marker to support CRS and SIT chronologies. Environ Pollut 129:31–37

Abril JM (2011) Could bulk density profiles provide information on recent sedimentation rates? J Paleolimnol 46:173–186

Abril JM, Fraga E (1996) Some physical and chemical features of the variability of k_d distribution coefficients for radionuclides. J Environ Radioact 30:253–270

Abril JM, Gharbi F (2012) Radiometric dating of recent sediments: beyond the boundary conditions. J Paleolimnol 48:449–460

Abril JM, García-León M, García-Tenorio R, Sánchez CI, El-Daoushy F (1992) Dating of marine sediments by an incomplete mixing model. J Environ Radioact 15:135–151

Akritas MG, Bershady MA (1996) Linear regression for astronomical data with measurement errors and intrinsic scatter. Astrophys J 470:706–714

Appleby PG (1998) Dating recent sediments by ^{210}Pb: problems and solutions. In: Illus E (ed) Dating of sediments and determination of sedimentation rate. STUK A-145, Finland, pp 7–24

Appleby PG (2001) Chronostratigraphic techniques in recent sediments. In: Last WL, Smol JP (eds) Tracking environmental change using lake sediments. Basin analysis, coring, and chronological techniques. Developments in paleoenvironmental research. Kluwer, Dordrecht, pp 171–203

Appleby PG, Oldfield F (1978) The calculation of lead-210 dates assuming a constant rate of supply of unsupported ^{210}Pb to the sediment. Catena 5:1–8

Appleby PG, Oldfield F, Thompson R, Huttunen P, Tolonen K (1979) Pb-210 dating of annually laminated lake sediments from Finland. Nature 280:53–55

Brunskill GJ (1969) Fayetteville Green Lake, New York. II. Precipitation and sedimentation of calcite in a meromictic lake with laminated sediments. Limnol Oceanogr 14:830–847

Brunskill GJ, Ludlam SD (1988) The variation of annual ^{210}Pb flux to varved sediments of Fayetteville Green Lake, New York from 1885 to 1965. Ver Internat Verein Limnol 23:848–854

Brunskill GJ, Ludlam SD, Peng T-H (1984) Mass balance and sedimentation of 137-Cs in Fayetteville Green Lake, N.Y. Chem Geol 44:101–117

Caroll J, Lerche I (2003) Sedimentary processes: quantification using radionuclides. Elsevier, Oxford

Christensen ER (1982) A model for radionuclides in sediments influenced by mixing and compaction. J Geophys Res 87:566–572

Chutko KJ, Lamoureux SF (2009) Biolaminated sedimentation in a High Arctic freshwater lake. Sedimentology 56:1642–1654

Di Gregorio DE, Fernández Niello JO, Huck H, Somacal H, Curutchet G (2007) ^{210}Pb dating of sediments in a heavily contaminated drainage channel to the La Plata estuary in Buenos Aires, Argentina. Appl Radiat Isotopes 65:126–130

Díaz-Asencio M, Alonso-Hernández CM, Bolanos-Álvarez Y, Gómez-Batista M, Pinto V, Morabito R, Hernández-Albernas JI, Eriksson M, Sánchez-Cabeza JA (2009) One century sedimentary record of Hg and Pb pollution in the Sagua estuary (Cuba) derived from ^{210}Pb and ^{137}Cs chronology. Mar Pollut Bull 59:108–115

El-Dahoushy F (1988) A summary of the lead-210 cycle in nature and related applications in Scandinavia. Environ Int 14:305–319

Emeis KC, Struck U, Leipe T, Pollehne F, Kunzendorf H, Christiansen C (2000) Changes in the C, N, P burial rates in some Baltic Sea sediments over the last 150 years—relevance to P regeneration rates and the phosphorus cycle. Mar Geol 167:43–59

Finsinger W, Bigler Ch, Krähenbühl U, Lotter AF, Ammann B (2006) Human impacts and eutrophication patterns during the past ~200 years at Lago Grande di Avigliana (N. Italy). J Paleolimnol 36:55–67

Goldberg ED (1963) Geochronology with Pb-210. Proceedings of a Symposium of Radioactive Dating, International Atomic Energy Agency, Vienna, pp 121–131

Graustein WC, Turekian KK (1986) ^{210}Pb and ^{137}Cs in air and soils measure the rate and vertical profile of aerosol scavenging. J Geophys Res 91(D13):14355–14366

Honeyman BD, Santschi PH (1989) A Brownian-pumping model for trace metal scavenging: evidence from Th isotopes. J Mar Res 47:951–992

Kerfoot WC, Robbins JA (1999) Nearshore regions of Lake Superior: multi-element signatures of mining discharges

and a test of Pb-210 deposition under conditions of variable sediment mass flux. J Great Lakes Res 25:697–720

Klaminder JP, Appleby JP, Crook P, Renberg I (2012) Post-deposition diffusion of 137Cs in lake sediment: implications for radiocaesium dating. Sedimentology 59:2259–2267

Koide M, Soutar A, Goldberg ED (1972) Marine geochronology with ^{210}Pb. Earth Planet Sci Lett 14:442–446

Koide M, Bruland K, Goldberg ED (1973) Th-228/Th-232 and Pb-210 geochronologies in marine and lake sediments. Geochim Cosmochim Acta 37:1171–1187

Krishnaswamy S, Lal D, Martin JM, Meybek M (1971) Geochronology of lake sediments. Earth Planet Sci Lett 11:407–414

Laissaoui A, Benmansour M, Ziad N, Ibn Majah M, Abril JM, Mulsow S (2008) Anthropogenic radionuclides in the water column and a sediment core from the Alboran Sea: application to radiometric dating and reconstruction of historical water column radionuclide concentration. J Paleolimnol 40:823–833

Lamoureux SF (1998) Distinguishing between the geomorphic and hydro-meteorological controls recorded in clastic varved sediments. Ph D. thesis, Department of Earth and Atrnospheric Sciences, University of Alberta, Canada

Lima AL, Hubeny JB, Reddy ChM, King JW, Hughen KA, Eglinton TI (2005) High-resolution historical records from Pettaquamscutt River basin sediments: 1. ^{210}Pb and varve chronologies validate record of ^{137}Cs released by the Chernobyl accident. Geochim Cosmochim Acta 69:1803–1812

Ludlam SD (1969) Fayetteville Green Lake, New York. III. The laminated sediments. Limnol Oceanogr 14:848–857

Ludlam SD (1974) Fayetteville Green Lake, NY VI. The role of turbidity currents in lake sedimentation. Limnol Oceanogr 19:656–664

Ludlam SD (1981) Sedimentation rates in Fayetteville Green Lake, N. Y, USA. Sedimentology 28:85–96

Ludlam SD (1984) Fayetteville Green Lake, N. Y. VII. Varve chronology and sediment focusing. Chem Geol 44:85–100

Nozaki Y, McMaster DJ, Lewis DM, Turekian KK (1978) Atmospheric Pb-210 fluxes determined from soil profiles. J Geophys Res 83:4047–4051

Nyffeler UP, Li YH, Santschi PH (1984) A kinetic approach to describe trace element distribution between particles and solution in natural aquatic systems. Geochim Cosmochim Acta 48:1513–1522

Ojala AEK, Francus P, Zolitschka B, Besonen M, Lamoureux SF (2012) Characteristics of sedimentary varve chronologies—a review. Quaternary Sci Rev 43:45–60

Rangarajan C, Madhavan R, Gopalakrishnan Smt S (1986) Spatial and temporal distribution of lead-210 in the surface layers of the atmosphere. J Environ Radioact 3:23–33

Reinikainen P, Meriläinen JJ, Virtanen A, Veijola H, Äystö J (1997) Accuracy of ^{210}Pb dating in two annually laminated lake sediments with high Cs background. Appl Radiat Isotopes 48:1009–1019

Robbins JA (1978) Geochemical and Geophysical applications of radioactive lead isotopes. In: Nriago JP (ed) Biochemistry of lead in the environment. Elsevier, Amsterdam, pp 285–393

Robbins JA, Edgington DN (1975) Determination of recent sedimentation rates in Lake Michigan using ^{210}Pb and ^{137}Cs. Geochim Cosmochim Ac 39:285–304

Robbins JA, Krezoski JR, Mozley SC (1977) Radioactivity in sediments of the Great Lakes; Post-depositional redistribution by deposit-feeding organisms. Earth Planet Sci Lett 36:325–333

Schettler G, Mingram J, Negendank JFW, Jiaqi L (2006a) Paleovariations in the East-Asian Monsson regime geochemically recorded in varved sediments of Lake Sihailongwan (Northeast China, Jilin province). Part 2: a 200-year record of atmospheric lead-210 flux variations and its palaeoclimatic implications. J Paeolimnol 35:271–288

Schettler G, Qiang L, Mingram J, Negendank JFW (2006b) Paleovariations in the East-Asian Monsson regime geochemically recorded in varved sediments of Lake Sihailongwan (Northeast China, Jilin province). Part 1: Hydrological conditions and flux. J Paleolimnol 35:239–270

Shanahan TM, Overpeck JT, Beck JW, Wheeler CW, Peck JA, King JW, Scholz ChA (2008) The formation of biogeochemical laminations in Lake Bosumtwi, Ghana, and their usefulness as indicators of past environmental changes. J Paleolimnol 40:339–355

Smith JN (2001) Why should we believe ^{210}Pb sediment geochronologies? J Environ Radioact 55:121–123

Smith JN, Boudreau BP, Noshkin V (1986) Plutonium and ^{210}Pb distributions in northeast Atlantic sediments: subsurface anomalies caused by non-local mixing. Earth Planet Sci Lett 81:15–28

Stevenson AC, Battarbee RW (1991) Palaeoecological and documentary records of recent environmental change in Garaet El Ichkeul: a seasonally Saline Lake in NW Tunisia. Biol Conserv 58:275–295

Trabelsi Y, Gharbi F, El Ghali A, Oueslati M, Samaali M, Abdelli W, Baccouche S, Ben Tekaya M, Benmansour M, Mabit L, Ben M'Barek N, Reguigui N, Abril JM (2012) Recent sedimentation rates in Garaet El Ichkeul Lake, NW Tunisia, as affected by the construction of dams and a regulatory sluice. J Soil Sediment 12:784–796

Turekian KK, Nozaki Y, Benninger LK (1977) Geochemistry of atmospheric radon and radon products. Annu Rev Earth Planet Sci 5:227–255

Tylmann W, Enters D, Kinder M, Moska P, Ohlendorf Ch, Poreba G, Zolitschka B (2013) Multiple dating of varved sediments from Lake Łazduny, northern Poland: toward an improved chronology for the last 150 years. Quat Geochronol 15:98–107

Tylmann W, Fischer HW, Enters D, Kinder M, Moska P, Ohlendorf Ch, Poreba G, Zolitschka B (2014) Reply to the comment by F. Gharbi on "Multiple dating of varved sediments from Lake Łazduny, northern Poland: toward an improved chronology for the last 150 years". Quat Geochronol 20:11–113

von Gunten HR, Moser RN (1993) How reliable is the ^{210}Pb dating method? Old and new results from Switzerland. J Paleolimnol 9:161–178

Wan GJ, Santschi PH, Sturm M, Farrenkothen K, Lueck A, Werth E, Schuler Ch (1987) Natural (^{210}Pb, ^{7}Be) and fallout (^{137}Cs, ^{239,240}Pu, ^{90}Sr) radionuclides as geochemical tracers of sedimentation in Greifensee, Switzerland. Chem Geol 63:181–196

Winkler R, Rosner G (2000) Seasonal and long-term variation of ^{210}Pb concentration in air, atmospheric deposition rate and

total deposition velocity in south Germany. Sci Total Environ 263:57–68

Wolfe B, Kling HJ, Brunskill GJ, Wilkinson P (1994) Multiple dating of a Freeze Core from Lake 227, and experimentally fertilized Lake with Varved sediments. Can J Fish Aquat Sci 51:2274–2285

Zaborska A, Carroll J, Papucci C, Torricelli L, Carroll ML, Walkusz-Miotk J, Pempkowiak J (2008) Recent sediment accumulation rates for the Western margin of the Barents Sea. Deep-Sea Res Pt II 55:2352–2360